Structure *18*

Supplemental Information

Polycomb Group Targeting through Different Binding Partners of RING1B C-Terminal Domain

Renjing Wang, Alexander B. Taylor, Belinda Z. Leal, Linda V. Chadwell, Udayar Ilangovan, Angela K. Robinson, Virgil Schirf, P. John Hart, Eileen M. Lafer, Borries Demeler, Andrew P. Hinck, Donald G. McEwen, and Chongwoo A. Kim

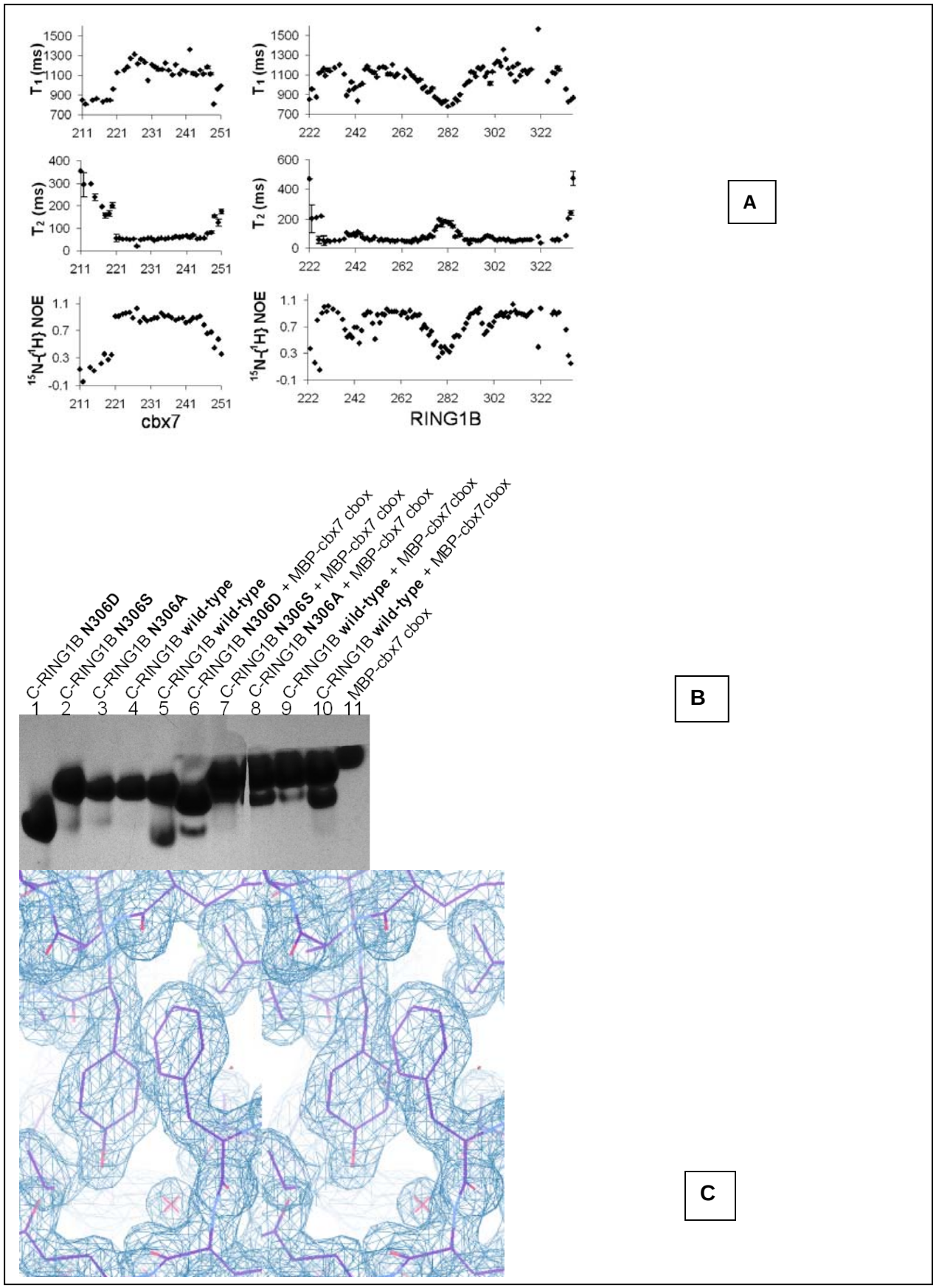

Figure S1. C-RING1B/cbx7 cbox conformational dynamics and structure

(**A**) Backbone conformational dynamics of the C-RING1B/cbx7 cbox complex. T_1, T_2, and ^{15}N-$\{^1H\}$ NOEs for cbx7 211 – 251 and for RING1B residues 222 – 336. The error bars for the T_1 and T_2 relaxation times are calculated by Monte Carlo sampling methods. Using an ^{15}N and ^{13}C labeled 1 mM complex (see Table S1 for a list of all proteins used in this study), we first assigned backbone atoms (^1HN, ^{15}N, ^{13}CO, $^{13}C^{\beta}$, $^{13}C^{\alpha}$) and then proceeded to measure the ^{15}N HSQC based longitudinal (T_1) and transverse (T_2) relaxation times along with the ^{15}N-$\{^1H\}$ heteronuclear Overhauser effects (^{15}N-$\{^1H\}$ NOE) on the ^{15}N labeled sample. The relaxation measurements show a stretch of approximately 30 residues within cbx7 that is highly ordered when in complex with C-RING1B. The long T_1 and short T_2 measurements along with the high ^{15}N-$\{^1H\}$ NOE values within cbx7 residues 219 – 248 compared to the residues at each termini indicate a well-ordered structure. The regions of disorder within C-RING1B precisely correspond to gaps in the sequence alignment between the RING orthologs (Fig. 1B). The areas of disorder observed in these NMR relaxation measurements are consistent with the structure of the complex (Fig. 1C – E).

(**B**) C-RING1B Asn 306 mutants bind the cbox domain. A native electrophoresis binding assay is shown. The difference in the two wild-type C-RING1B proteins (lanes 4 and 5) shows the heterogeneity that can stem from Asn deamidation. The lane 4 wild-type differs from the lane 5 wild-type in that lane 4 is a more recent prep and additional cation exchange chromatography was performed. Lane 5 wild-type shows a significant fraction of the protein sample migrating faster in the gel and similar to the rate of the Asn306Asp mutant. This band likely corresponds to a deamidated protein because a single Asn deamindated protein and the Asn306Asp mutant would have the same charge and be nearly identical in molecular weight.

(**C**) Sample electron density of the C-RING1B/cbx7 219 – 248 crystal structure. Stereoview of the 1.7 Å, 2Fo – Fc map contoured at 1σ. The map is centered at the cbx7 Phe 234 base stacking interaction with C-RING1B Tyr 262.

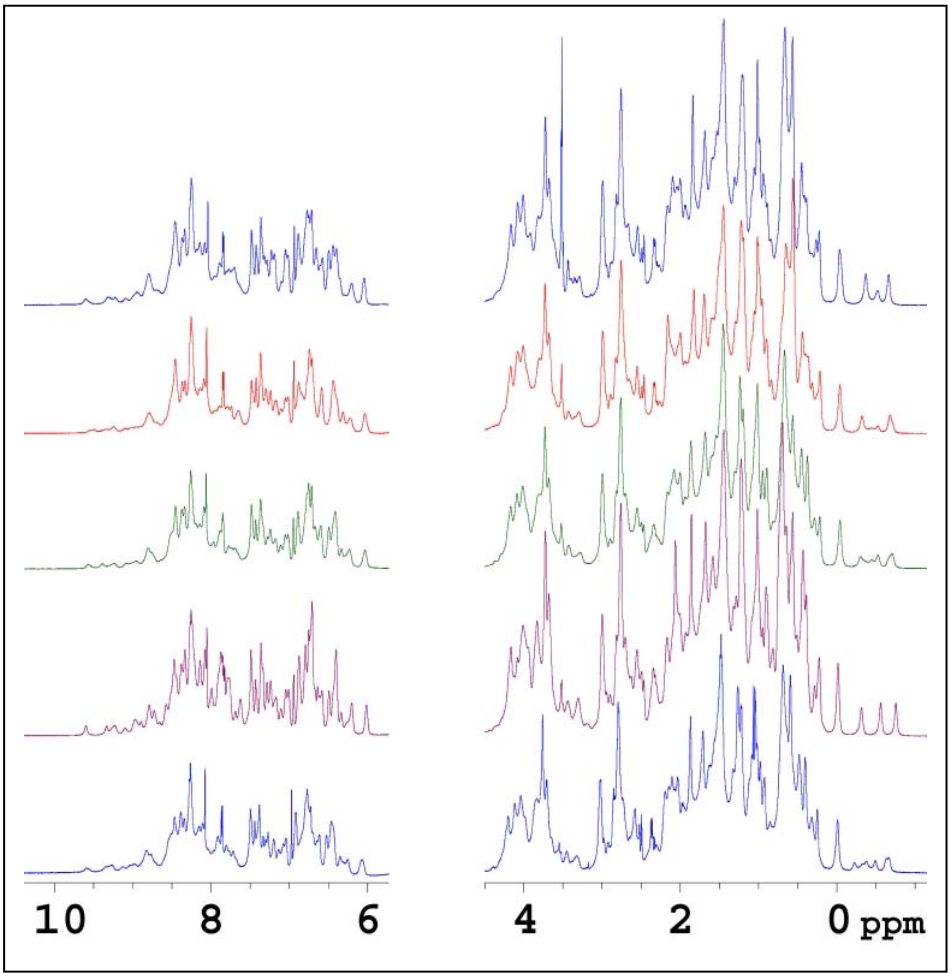

Figure S2. 1D ^{1}H NMR spectra of wild-type C-RING1B and the structure guided C-RING1B mutants used in the binding studies
The spectra aligned from top to bottom are Val229Ala, Tyr247Ala, His258Ala, Tyr262Ala, and wild-type.

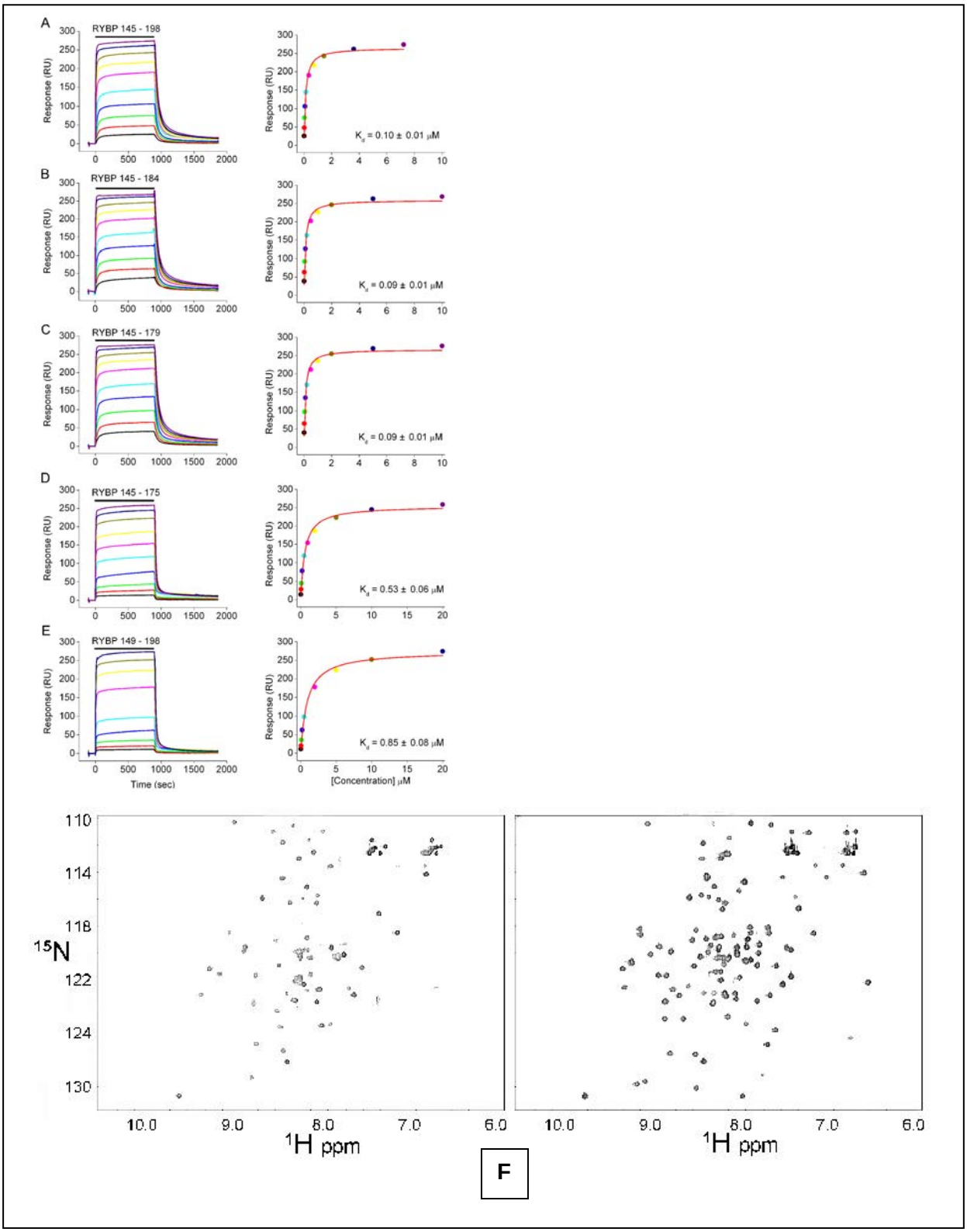

Figure S3. C-RING1B/RYBP interaction

(**A - E**) Determination of the minimal binding region of RYBP required to bind C-RING1B using surface plasmon resonance (SPR). Data for each variant are shown in the indicated panel (**A - E**). In each panel, the plot on the left is an overlay of the sensorgrams for a representative concentration series. The black bar marks when the indicated RYBP variant was injected. The plot on the right shows the response at equilibrium as a function of MBP-RYBP protein concentration. The color of each data point in the plot on the right, corresponds to the trace of identical color in the plot on the left. The data were fit to a hyperbolic equation (red lines), and the K_d values indicated are the mean value from experiments performed on two different surfaces, while the standard deviation was calculated by descriptive statistics using Origin 7 software. The SPR data clearly identifies RYBP residues 145 – 179 as the minimum binding region for maintaining the high affinity with C-RING1B (K_d = 90 nM). These residues include both a beta sheet that is similar to the cbx7 cbox domain, and a loop structure that is completely different than the cbx7 cbox loop (Fig. 3E). Thus, in addition to identifying the minimum binding region, the SPR data also shows that both the beta sheet and loop structures are required to maintain a stable complex with C-RING1B.
(**F**) ^{5}N-^{1}H HSQC of ^{15}N labeled C-RING1B alone (150 μM) (left) and with 1.5 molar equivalents of non-labeled RYBP 145 – 179 added to the same sample (right).

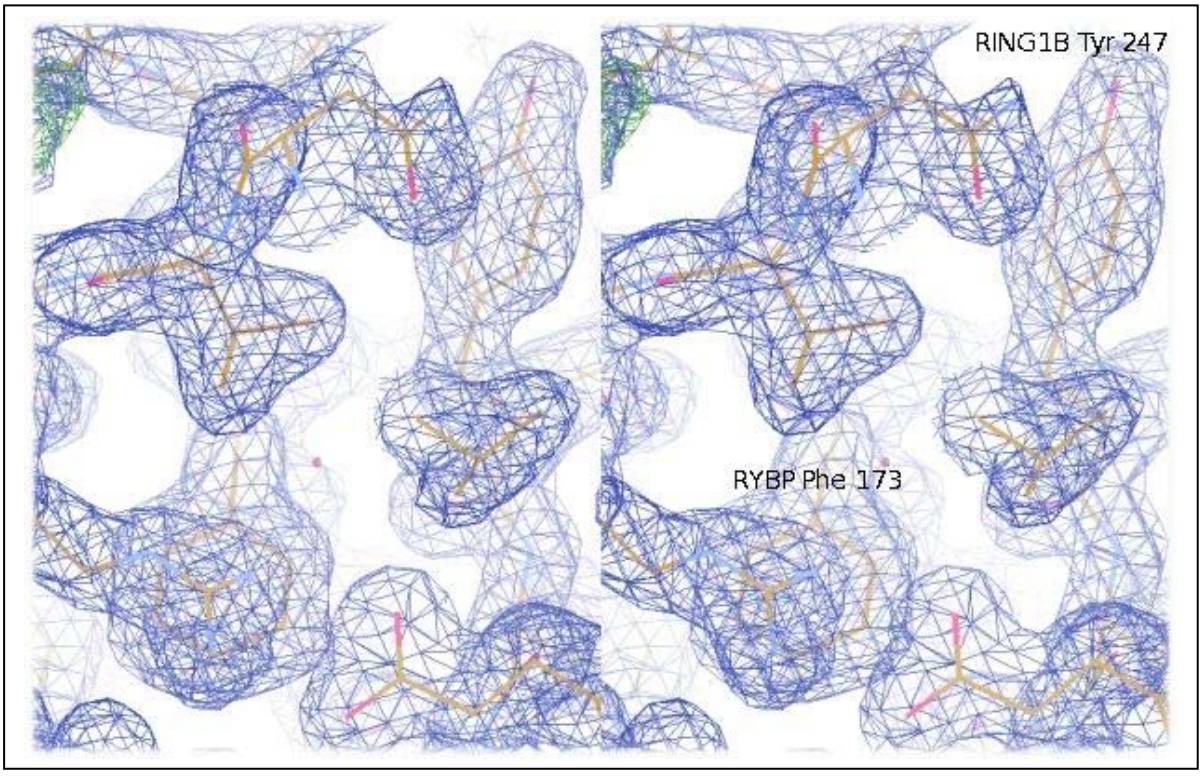

Figure S4. Stereo view of the 1.7 Å, 2Fo – Fc map contoured at 1σ of the RYBP loop interaction There are six C-RING1B/RYBP complexes in the asymmetric unit. All descriptions in the text were of a C-RING1B/RYBP complex with the best electron density

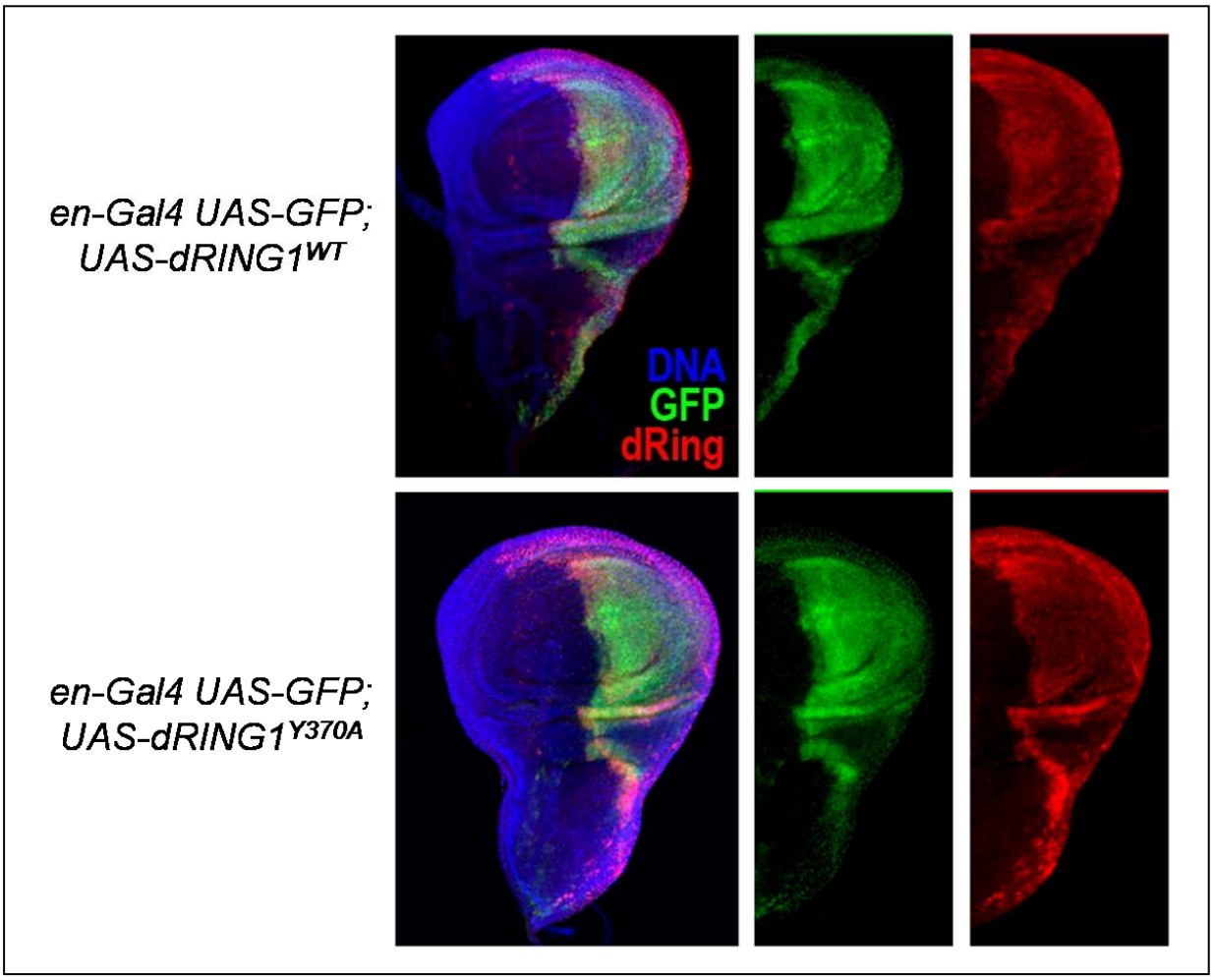

Figure S5. Wing disc images of the transgenic flies
Expression of the *dRING1* exogenous gene products in the posterior compartment of the wing disc is accomplished through the *engrailed Gal4* driver (*en-Gal4*) which results in the expression of both *GFP* and *dRING1* genes that are inserted into two different chromosomal locations and are under control of the Gal4 upstream activating sequence (UAS). Blue hoechst dye stains DNA and is used to highlight the entire wing disc.

Table S1. Protein constructs used for in vitro experiments.

ID	Experiment	Figures	N-terminal leader sequence	protein	C-ter sequence	Additional notes
1	NMR, Ultracentrifugation	S1A, 3A	MEKTR	RING1B 222-336	SRD	^{13}C, ^{15}N for assignments, ^{15}N only for Figs. S1A and 3A.
2	Crystallography	1C-E, 4, S1C, S4	M	RING1B 223-333		N306D
3	Ultracentrifugation, Native gel, NMR	2A, 2B, 3B, S1B, S2	MHHHHHHAMENLYFQ*GTR	RING1B 222-336	SRD	
4	NMR, SPR	S3B, S3A	MEKTR	RING1B 222-336	SRHHHHHH	^{15}N labeled for NMR
5	NMR	S1A	MEKTR	cbx7 211-251	SRHHHHHH	^{15}N labeled
6	Crystallography	1C-E, S1C	MHHHHHHGVDSPSAELDKKAENLYFQ*GTR	cbx7 219-248		
7	Native gel	2A, 2B, S1B	MBP-AMEKTRES	cbx7 211-251	SRH	
8	Native gel	2B	MBP-AMEKTRES	cbx7 211-240		
9	Native gel	3B	MBP-AMETRAYG	YAF2 103-150	SRH	
10	Ultracentrifugation	3A	MEKT	RYBP 145-198	SRHHHHHH	^{15}N labeled
11	SPR	S3, 3C	MBP-AMET	RYBP 145-198		
12	SPR	S3, 3C	MBP-AMET	RYBP 145-184		
13	SPR	S3, 3C	MBP-AMET	RYBP 145-179		
14	SPR	S3, 3C	MBP-AMET	RYBP 145-175		
15	SPR	S3, 3C	MBP-AMETR	RYBP 149-179		
16	Crystallography, NMR	3D, 3E, S4	MHHHHHHGVDSPSAELDKKAENLYFQ*GT	RYBP 145-179		Construct not cleaved with TEV for Fig.3D and 3E.

All sequences are from human proteins. Mass spectrometry analysis of construct ID #2 indicated the processing of the initial Met residue thus leaving just the RING1B residues 223 – 333. Figure numbers with an S prefix indicates Supplementary Figures. * = TEV cleavage site. For all MBP fusion constructs, the 5' end of the genes were sub-cloned into the NcoI site of pBADM-41+ (EMBL) and corresponds to the AM residues in the sequence.

SUPPLEMENTAL EXPERIMENTAL PROCEDURES

X-ray crystallography

C-RING1B/cbx7 219 – 248

A single crystal that grew from an initial screen condition composed of 0.1 M MES pH 6.5, 25% PEG monomethyl ether 550, 10 mM $ZnSO_4$ was used to collect an initial native dataset. The crystal used for the iodine heavy atom derivative was grown using 43 mg/ml protein concentration and a well solution containing 50 mM tris-HCl pH 7.2, 25% PEG 1.5K, 200 mM Li_2SO_4, 10 mM $ZnSO_4$. The iodide was incorporated by placing the crystal in a cryo protectant composed of the well solution with added 5% glycerol and 0.44 M LiI. Fully incorporated selenomethionine (Van Duyne, et al., 1993) (Se-Met) crystals were grown by setting up a hanging drop with 1 μl of 43 mg/ml of the Se-Met protein sample which contained 5% glycerol, mixed with an equal volume of 50 mM MES pH 6.6, 28% PEG 4000, 50 mM NaOAc, 50 mM Zn_2SO_4 and immediately seeding the drop by adding a 0.2 μl of a microseed stock solution.

C-RING1B/RYBP 145 – 179

The native C-RING1B Asn306Asp/RYBP complex crystals grew in 32% PEG 1750, 0.125 M lithium sulfate, 10% ethylene glycol and 0.05 M CHES at pH 8.0. The Se-Met derivative crystals grew in 32% PEG 2000, 0.09 M lithium sulfate, 12% ethylene glycol and 0.075M CHES at pH 8.0.

NMR Methods

All samples were prepared to 0.35 mM. The spectra were collected on a Bruker Av600 at 300 K.

Surface Plasmon Resonance methods

All surface plasmon resonance (SPR) data were collected at room temperature using a Biacore 3000 instrument. C-RING1B was immobilized on a sensor chip CM5 (GE Healthcare) at two different densities (160 and 120 response units (RU)) using amine-coupling chemistry (Biacore Inc. amine coupling kit). A concentration series of the indicated MBP-RYBP fusion protein was flowed over the chip at 5 μl/min in 10 mM HEPES pH 7.4, 150 mM NaCl, 3 mM EDTA, 0.005% Surfactant P20 running buffer until an equilibrium response was reached. Two 5 μl injections of guanidinium hydrochloride were used to regenerate the chip surfaces after each injection. Ten buffer injections were performed to stabilize the instrument before introducing the MBP-RYBP proteins to the mobile phase, and an additional three buffer injections were randomly dispersed with the experimental samples. Data were double referenced by first subtracting the responses on a reference flow cell, and then subtracting the responses from the averaged blank buffer injections utilizing Scrubber 2 software. Plots were made of the response at equilibrium as a function of MBP-RYBP concentration, and fit to a hyperbolic equation to obtain the equilibrium dissociation constants utilizing Origin 7 Software.

Analytical Ultracentrifugation Methods

Hydrodynamic corrections for buffer conditions were made according to data published by Laue *et al.* (Laue, et al., 1992) and as implemented in UltraScan. The sedimentation experiments were performed at 20° C in standard 2-channel centerpieces. The data were analyzed and time-invariant noise was subtracted with the 2-dimensional spectrum analysis (Brookes, et al., 2010).

Noise-corrected data were analyzed with the enhanced van Holde - Weischet analysis (Demeler and van Holde, 2004).

SUPPLEMENTAL REFERENCES

Brookes, E., Cao, W., and Demeler, B. (2010). A two-dimensional spectrum analysis for sedimentation velocity experiments of mixtures with heterogeneity in molecular weight and shape. Eur. Biophys. J. 39, 405-414.

Demeler, B., and van Holde, K.E. (2004). Sedimentation velocity analysis of highly heterogeneous systems. Anal. Biochem. 335, 279-288.

Laue, T.M., Shah, B.D., Ridgeway, T.M., and Pelletier, S.L. (1992). Computer-aided interpretation of analytical sedimentation data for proteins. In *Analytical Ultracentrifugation in Biochemistry and Polymer Science*, Harding, S. E., Rowe, A. J. and Horton, J. C. eds., Cambridge, Royal Society of Chemistry) pp. 90-125.

Van Duyne, G.D., Standaert, R.F., Karplus, P.A., Schreiber, S.L., and Clardy, J. (1993). Atomic structures of the human immunophilin FKBP-12 complexes with FK506 and rapamycin. J. Mol. Biol. 229, 105-124.